

Energy landscape diversity and supercooled liquid properties

Frank H. Stillinger

Princeton Materials Institute, Princeton University, Princeton, New Jersey 08544

Pablo G. Debenedetti

Department of Chemical Engineering, Princeton University, Princeton, New Jersey 08544

(Received 12 September 2001; accepted 19 November 2001)

Families of model “rugged landscape” potential energy functions have been constructed and examined, in order to clarify the molecular-level basis for the relationship between thermodynamic and kinetic behaviors of glassforming substances. The general approach starts by forming elementary basin units, each of which contains a single local minimum (inherent structure). These units are then spliced together to create a continuous composite potential with the requisite number of basins, upper and lower limits, and boundary conditions. We demonstrate by example that this approach creates wide topographic diversity. Specifically, many pairs of model potential functions exist that share identical thermodynamic properties (depth distribution of minima), but drastically different kinetics (overall topography). Thus, within the confines of this purely mathematical exercise, the “strong” versus “fragile” classifications of thermodynamics and of kinetics are logically disconnected. We conclude that the empirically-observed correlation between thermodynamic and kinetic behaviors embodied, for example, in the Adam–Gibbs equation, must rest upon an additional physical principle involving details of interparticle interactions, transcending the purely mathematical aspects of potential energy landscape topography. © 2002 American Institute of Physics. [DOI: 10.1063/1.1434997]

I. INTRODUCTION

The ability of all substances to form condensed phases, and the static and dynamic properties of those phases, depend fundamentally upon the interactions operating among the constituent particles (atoms, ions, or molecules). In particular this is true for liquids that readily supercool toward, and into, the glass state. Despite the existence of an enormous literature devoted to supercooled liquids and their glasses,^{1–3} scientific insight in this area remains incomplete. The present theoretical contribution identifies and attempts to clarify one of these knowledge gaps.

It has become customary to invoke Angell’s empirical classification scheme for glass forming substances, placing each on a one-dimensional scale between “strong” and “fragile” extremes.⁴ Examples of the former typically exhibit little difference between liquid and crystal heat capacities C_p , and tend to have viscosities and mean relaxation times described well by an Arrhenius function of temperature. Examples of the latter have liquid heat capacities that are significantly larger than the corresponding crystal values, by a margin that increases with extent of supercooling; and the viscosities and mean relaxation times display “super-Arrhenius” behavior (strong upward curvature of logarithmic plots vs inverse temperature).

The calorimetric behavior of the fragile glassformers (e.g., ortho-terphenyl), historically lies at the heart of the so-called “Kauzmann paradox.”⁵ The supercooled-liquid vs crystal heat capacity discrepancy, when extrapolated below the point of dynamical arrest at the experimental glass transition, suggests that the entropy of the configurationally disordered liquid would cross that of the ordered crystal at some

positive temperature T_K ; furthermore, extrapolation to absolute zero temperature appears to imply that the metastable liquid would possess lower entropy than that of the crystal. This last implication violates the third law of thermodynamics.⁶ The fact that this impending violation is thwarted by the kinetically-controlled experimental glass transition suggests a possible connection between the thermodynamics and the kinetics of supercooled liquids.

One of the more frequently cited suggestions for avoiding this paradox is that an “ideal glass transition” intervenes at, or close to, the Kauzmann temperature T_K .⁷ This hypothetical scenario postulates that if full structural relaxation could be maintained for the substance involved, the supercooling would yield the unique optimal (i.e., lowest energy) amorphous structure at this positive temperature. It should be noted in passing that theoretical objections to this ideal glass transition concept have been raised,⁸ and alternative scenarios for avoiding the third-law violation have been advanced.^{8–10}

Adam and Gibbs¹¹ originated an early attempt to link quantitatively the thermodynamic behavior of supercooled liquids to their flow and relaxation kinetics. These authors introduced and exploited the concept of elementary “cooperatively rearranging regions” in the low temperature liquid to establish this connection. Their analysis produced the following generic expression connecting shear viscosity η , or alternatively a mean relaxation time τ , to the configurational entropy per particle S_{conf} of the supercooled liquid,

$$\eta(T), \tau(T) \cong A \exp[B/TS_{\text{conf}}(T)]. \quad (1.1)$$

Here A and B are suitable temperature-independent multipli-

ers. If indeed a given fragile glassformer possesses a Kauzmann temperature $T_K > 0$, and if S_{conf} vanishes at this point, then the Adam–Gibbs expression (1.1) predicts non-Arrhenius behavior for η and τ , with both diverging to infinity at that temperature. In the Adam–Gibbs theory S_{conf} is that portion of the entropy attributable to the “rugged landscape” character of the system’s potential energy function. Although the original derivation referred to isobaric conditions, the conclusions are unchanged if instead number density is fixed.

Although the concept of “cooperatively rearranging regions” has consistently remained innocent of precise definition, the Adam–Gibbs expression (1.1) has enjoyed appreciable success at correlating static and dynamic measurements for a substantial range of glass formers.¹² This success has emboldened several authors to attempt an explanation, or rationale, in terms of the multidimensional potential energy surface, and its topographic “rugged landscape” characteristics.^{13–16} The present paper addresses this last viewpoint, utilizing families of model potential energy functions and their corresponding statistical mechanical analyses.

Section II contains a brief review of the basic properties of many-body potential energy functions, as they pertain to supercooling and glass transition phenomena. This review includes the transformation of partition functions to the basin-based inherent structure representation.^{17–19} Section III introduces a family of “rugged” one-dimensional potential energy functions that are composed piecewise out of modular single basin units. The form of the modular units and their rules for combination lead to a simple version of the inherent structure representation for thermodynamic properties. Section IV exposes a fundamental, and somewhat iconoclastic, property of these one-dimensional rugged landscapes. Specifically, it is possible to identify pairs of functions that produce identical thermodynamic properties, yet have very different dynamics-controlling topographies, thus implying a logical disconnection between the two aspects. This latter observation is not restricted to simple one-dimensional model potentials. Section V offers several generalizations to higher-dimensional spaces that exhibit the same logical disconnection. The final Sec. VI discusses the need for a principle, not purely mathematical in nature, to explain the empirical connection between thermodynamic and kinetic properties of supercooled liquids, allowing both to be (at least approximately) placed together on the strong-to-fragile scale.

II. BASINS AND INHERENT STRUCTURES

Let $\mathbf{r}_1 \cdots \mathbf{r}_N$ be the configurational coordinates for N particles confined to volume V . Each \mathbf{r}_i will include internal degrees of freedom if nonspherical and/or structured particles are involved, otherwise they specify only center positions. The potential energy of interaction will be denoted by $\Phi(\mathbf{r}_1 \cdots \mathbf{r}_N)$. This function will be bounded below by a quantity proportional to N ,

$$\Phi(\mathbf{r}_1 \cdots \mathbf{r}_N) \geq CN, \quad (2.1)$$

for some suitable constant C . No analogous upper bound can be assigned on account of strong repulsions that act between

particles at small separations. Φ will be continuous and at least twice differentiable with respect to the components of $\mathbf{r}_1 \cdots \mathbf{r}_N$, provided no two particles have coincident nuclei.

The multidimensional “landscape” presented by the Φ hypersurface in the space of $\mathbf{r}_1 \cdots \mathbf{r}_N$ divides naturally into “basins,” each one of which contains a single embedded Φ minimum. The configuration at such a minimum is a mechanically stable arrangement of the system’s particles, and is usually denoted as an “inherent structure.” Each basin is defined to be the locus of points in the multidimensional configuration space that connect, or “drain,” to the minimum via steepest descent on the Φ hypersurface. Specific model calculations,^{20,21} as well as general arguments,²² indicate that for N identical particles, each with symmetry factor s , the number Ω of basins and inherent structures has the following asymptotic form for large N ,

$$\ln \Omega \sim \ln(N!s^N) + \alpha N. \quad (2.2)$$

Here, $\alpha > 0$ will be substance-specific, and will generally vary with number density N/V . The first term on the right-hand side of Eq. (2.2) is the logarithm of the number of equivalent symmetry sectors into which the multidimensional configuration space divides; parameter α expresses the exponential rise rate with N at which the number of geometrically distinguishable inherent structures increases.

Transition states (first-order saddle points) involved in the dynamics of switching between pairs of basins, lie within the shared boundaries for those basins. The energy of excitation from the inherent structure at the bottom of a basin to such a transition state is an $O(1)$ quantity, and there are typically $O(N)$ such simple exit channels from any basin. The difference in potential energy altitude,

$$\Phi(\text{highest}) - \Phi(\text{lowest}) \quad (2.3)$$

between the highest-lying and the lowest-lying inherent structures is also an $O(N)$ quantity. This requires that such a pair of extreme inherent structures must be widely separated in the configuration space, i.e., many $O(1)$ transitions are required to pass from one to the other.

For some purposes it is useful to classify basins by their depths, that is, by the potential energy values of their embedded inherent structures. In the large system limit ($N, V \rightarrow \infty$, N/V constant) the appropriate representation for the distribution generalizes Eq. (2.2) to the following:

$$\ln \Omega(\phi) \sim \ln(N!s^N) + \sigma(\phi)N, \quad (2.4)$$

where the intensive order parameter ϕ is Φ/N for the inherent structures, and $\sigma \geq 0$ is independent of N and is defined between finite lower and upper limits,

$$\Phi(\text{lowest})/N \equiv \phi_{\min} \leq \phi \leq \phi_{\max} \equiv \Phi(\text{highest})/N. \quad (2.5)$$

The connection between Eqs. (2.2) and (2.4) for the large-system limit is simply,

$$\alpha = \max_{\phi} [\sigma(\phi)]. \quad (2.6)$$

An intrabasin vibrational partition function may simply be defined by integrating the appropriate Boltzmann factor over the interior of that basin (B). For present purposes, the quantity of significance is the mean vibrational partition

function for those basins whose inherent structures lie in the immediate depth neighborhood of a given ϕ value. The corresponding vibrational free energy per particle, at inverse temperature $\beta=1/k_B T$, will be denoted by $f_{\text{vib}}(\beta, \phi)$,

$$\beta f_{\text{vib}}(\beta, \phi) \sim N^{-1} \ln \left\langle Y_N(\beta) \times \int_B \exp[-\beta \Delta \Phi(\mathbf{r})] d^{DN} \mathbf{r} \right\rangle_{\phi \pm \varepsilon}. \quad (2.7)$$

Here D is the space dimension of the system, $\Delta \Phi$ measures the potential energy rise within the basin B from its local minimum at the inherent structure, and $Y_N(\beta)$ is the partition function for all conjugate momenta. For structureless point particles $Y_N(\beta)$ reduces to λ_T^{-DN} , where $\lambda_T(\beta)$ is the mean thermal deBroglie wavelength for those point particles.

At fixed number density, the Helmholtz free energy emerges next as a variational minimum for an exceptionally simple linear combination involving σ and f_{vib} ,

$$\beta F(\beta) \sim N \min_{\phi} [\beta \phi - \sigma(\phi) + \beta f_{\text{vib}}(\beta, \phi)]. \quad (2.8)$$

The minimizing value of the order parameter, $\phi^*(\beta)$, locates the temperature-dependent depth of the dominating basins at the prevailing temperature. Expression (2.8) is strictly valid only in the large-system asymptotic limit, for which an integrand-maximum evaluation of the partition function becomes appropriate.¹⁷⁻¹⁹

In discussion of supercooling and glass formation, it is useful to modify the meaning of Eq. (2.8) to avoid interference by the crystallization transition. Conceptually, this is easily accomplished by defining σ and f_{vib} only for the ‘‘amorphous’’ subset of basins within the multidimensional configuration space.⁸ This subset contains the overwhelming majority of all basins, and determines the value of α in Eqs. (2.2) and (2.6). The result of this basin restriction is a precise definition of free energy F for the metastable supercooled liquid via Eq. (2.8). For the remainder of this paper we shall presume that this modification is in effect.

III. MODULAR BASIN UNITS

In the interests of simplicity and clarity, we restrict this initial portion of our analysis to rugged potential energy functions defined in just one space dimension. This suffices to introduce and to establish our main points. Various directions of generalization to the more physically relevant case of many dimensions form the subject of Sec. V.

Define the following pair of modular potential energy units over the interval $0 \leq x \leq 1$:

$$P(x|+1) = -(9/16)\cos(\pi x) + (1/2)\cos(2\pi x) + (1/16)\cos(3\pi x); \quad (3.1)$$

$$P(x|-1) \equiv P(1-x|+1) = (9/16)\cos(\pi x) + (1/2)\cos(2\pi x) - (1/16)\cos(3\pi x). \quad (3.2)$$

One easily verifies the following properties:

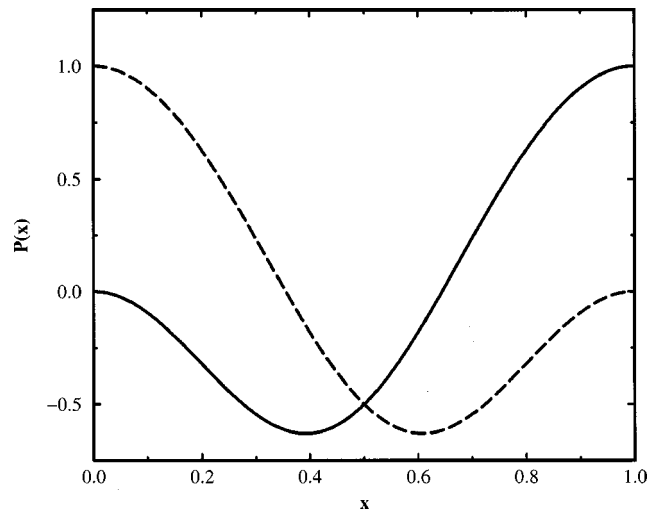


FIG. 1. Modular basin functions $P(x|\pm 1)$, used for construction of composite ‘‘rugged landscape’’ potential energy functions (Sec. III).

$$P(0|+1) = 0, \quad (3.3)$$

$$P(1|+1) = 1,$$

$$P'(0|+1) = P'(1|+1) = 0, \quad (3.4)$$

$$P''(0|+1) = P''(1|+1) = -2\pi^2. \quad (3.5)$$

In addition $P(x|+1)$ possesses a single interior minimum at $0 < x_{\text{min}} < 1$, where

$$\cos(\pi x_{\text{min}}) = 1/3,$$

$$x_{\text{min}} \cong 0.391\ 826\ 552, \quad (3.6)$$

$$P(x_{\text{min}}|+1) = -17/27,$$

and the curvature at this minimum is given by

$$P''(x_{\text{min}}|+1) = 20\pi^2/9. \quad (3.7)$$

Analogous results pertain to the mirror image function $P(x|-1)$.

Figure 1 illustrates the two modular unit functions. Each constitutes a single one-dimensional basin, with an interior minimum, and vanishing gradient at the endpoints. The net altitude change across such a basin is ± 1 , as indicated by the discrete index for the functions.

The next step is to use an ordered set of M of these modular units to form a multibasin rugged potential energy function. This can be accomplished by placing the units end to end, with vertical shifts to ensure continuity of the result across the seams. By construction, the first and second derivatives will also be continuous, yielding a reasonably smooth composite function.

Any given sequence of modular units used to form a composite function can be specified in an obvious way as a sequence of Ising spins $\mu_i = \pm 1$. The multibasin functions Φ of interest are defined over the interval $0 \leq x \leq M$, by means of the generic expression,

$$\Phi(x) = P(x-j+1|\mu_j) + \sum_{i=1}^{j-1} \mu_i + C(\mu_1 \cdots \mu_M),$$

$$(j-1 \leq x \leq j), \quad (3.8)$$

where in each case $C(\mu_1 \cdots \mu_M)$ will be chosen so that the absolute minimum of Φ is zero. We will require $\Phi(x)$ to satisfy periodic boundary conditions,

$$\Phi(M) = \Phi(0), \quad (3.9)$$

which in turn requires that

$$\sum_{i=1}^M \mu_i = 0. \quad (3.10)$$

In other words, the Ising sequence must contain equal numbers $M/2$ of positive and negative spins.

In spite of horizontal shifts, altitude adjustments, and mirror imaging, all basins comprised in the composite functions $\Phi(x)$, Eq. (3.8), basically have the same shape. Consequently the vibrational free energy f_{vib} is the same for all basins. On account of this special circumstance, the averaging shown earlier in Eq. (2.7) is unnecessary, and f_{vib} depends only on β , not ϕ . For this one-dimensional case, then, evaluation of vibrational free energy requires evaluation of only a single configurational integral,

$$R(\beta) = \int_0^1 \exp[-\beta P(x|+1) - 17\beta/27] dx. \quad (3.11)$$

One easily determines that $R(\beta)$ is a monotonically decreasing function of β , with low-temperature and high-temperature limiting forms as follows:

$$R(\beta) \sim 3/(10\pi\beta)^{1/2} \quad (\beta \rightarrow +\infty), \quad (3.12)$$

$$R(\beta) = 1 - 17\beta/27 + O(\beta^2) \quad (\beta \rightarrow 0). \quad (3.13)$$

On account of the ϕ independence of f_{vib} , the value $\phi^*(\beta)$ of this order parameter that identifies the dominant basins at any given temperature is now determined by the simple criterion,

$$\sigma'(\phi^*) = \beta. \quad (3.14)$$

This can be interpreted as locating the tangency point of a straight line with slope β that rolls on top of the $\sigma(\phi)$ curve.

If any one of the composite functions $\Phi(x)$, Eq. (3.8), is intended to represent the rugged landscape of an N -body system in one of its symmetry sectors, then one is motivated to set

$$M \cong \exp(\alpha N) \quad (3.15)$$

to be consistent with Eq. (2.2) above.

IV. TOPOGRAPHIC VARIABILITY AT FIXED DEPTH DISTRIBUTION

Given that equal numbers $M/2$ of Ising spins are $+1$ and -1 , the number of nominally distinct sequences of spins, and of the associated composite functions $\Phi(x)$, will formally be

$$M! / [(M/2)!]^2. \quad (4.1)$$

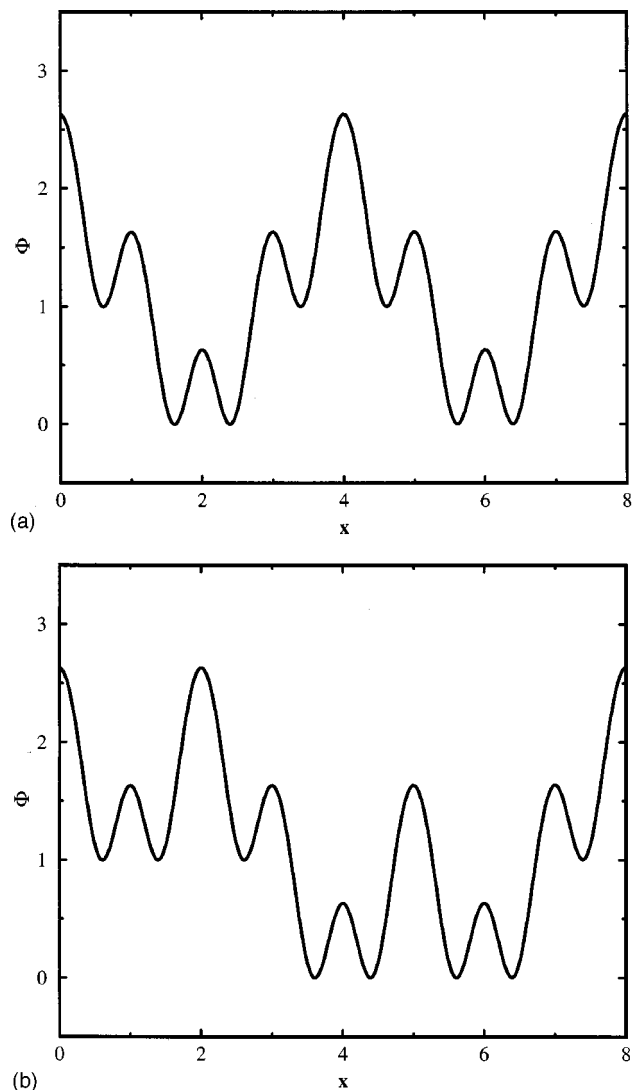


FIG. 2. The simplest pair of one-dimensional composite potentials that possess a common distribution of inherent structure depths (4 at 0, 4 at 1), but distinct topographies. Cases (a) and (b) refer, respectively, to Eqs. (4.2) and (4.3).

However many pairs of Φ 's in this set will be substantially the same, differing only by translation and/or reflection. Nevertheless this still leaves wide latitude for topographic diversity, even under the constraint of a fixed distribution of basin depths. The simplest case occurs for $M=8$, with 4 inherent structures each at $\Phi=0$ and at $\Phi=1$. The corresponding Ising spin representations are

$$-1, -1, +1, +1, -1, -1, +1, +1 \quad (4.2)$$

and

$$-1, +1, -1, -1, +1, -1, +1, +1. \quad (4.3)$$

Figure 2 illustrates these two contrasting examples that display distinct "landscape" profiles.

Experience shows that examples of such topographic diversity, subject to the constraint of a fixed depth distribution, rapidly proliferate as the number M of modular units in-

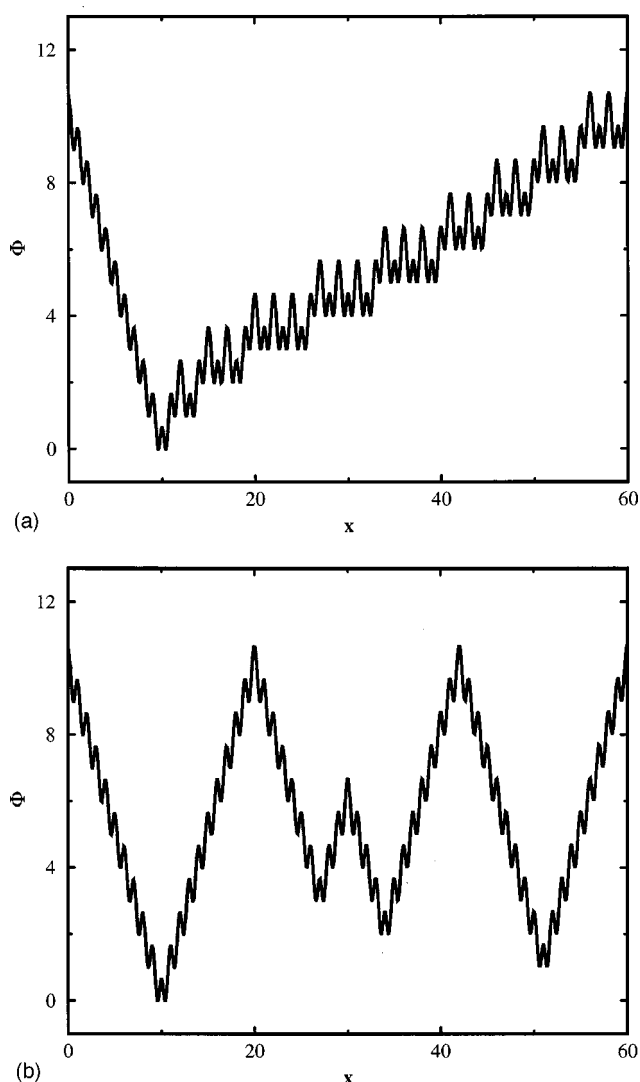


FIG. 3. Contrasting pair of $M = 60$ composite potentials, both possessing the basin depth distribution specified in Eq. (4.4).

creases. In fact, the number of distinguishable topographies that share a common basin depth distribution can also increase as M increases.

Figure 3 presents a strongly contrasting pair of composite functions for $M = 60$, using a schematic protocol for simplicity. For this pair, the basin depth distribution from bottom ($\Phi = 0$) to top ($\Phi = 9$) involves the following numbers:

$$2, 4, 6, 8, 8, 8, 6, 6, 6, 6. \quad (4.4)$$

The reader can easily verify that many other topographies exist with this same depth distribution. The example shown in Fig. 3(a) amounts to a single “metabasin,” or “funnel,” of the qualitative type often cited as relevant to the proper folding of proteins into their native forms. On the other hand, Fig. 3(b) exhibits a larger number of metabasins separated by high barriers that one can see would act as kinetic barriers to equilibration.

An alternative representation of rugged potential surfaces utilizes “disconnectivity graphs.” These have the advantage of explicitly showing the existence of kinetic pathways that connect different portions of the configuration

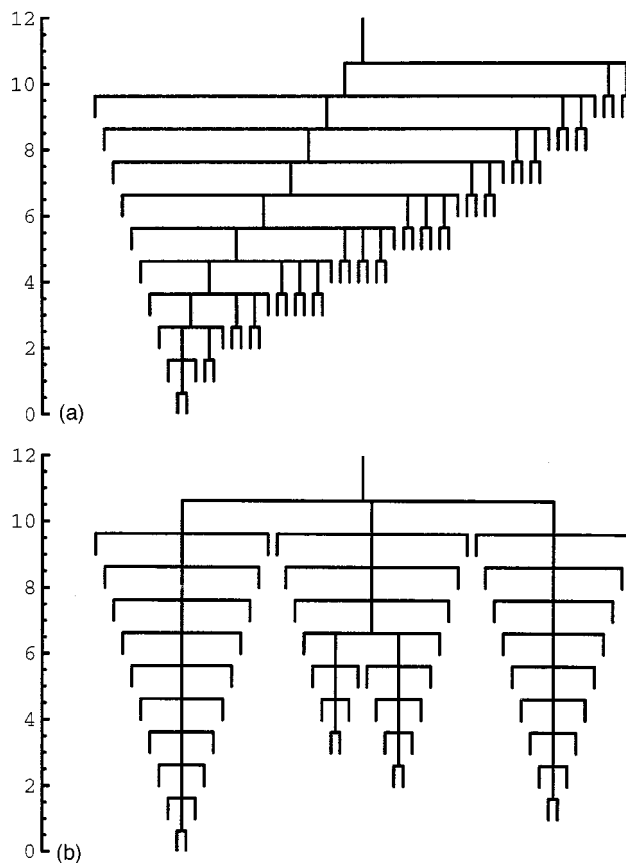


FIG. 4. Disconnectivity graphs for the pair of $M = 60$ composite potentials shown in Figs. 3(a) and 3(b), respectively.

space at any choice of total energy.^{23–25} Figures 4(a) and 4(b) present the disconnectivity graphs for the two surfaces in Figs. 3(a) and 3(b), respectively.

It is possible to state simple rules for transforming one M -unit Φ into another, without changing the depth distribution. The trivial rules of translation ($x \rightarrow x + n$) and reversal ($x \rightarrow M - x$) have already been noted. In addition, one has the following:

- (1) any connected subsequence of $M' < M$ modular units that begins and ends at the same Φ level may be reversed;
- (2) any pair of distinct subsequences, whose respective starting and ending Φ levels are pairwise equal, may be interchanged;
- (3) any pair of distinct connected subsequences, with the starting Φ level of each one equal to the ending Φ level of the other, may be interchanged after both are reversed.

All topographically distinct Φ 's possessing a common depth distribution can be generated from any one of them by repeated application of these rules.

In the large-system limit for which the logarithm of the depth distribution is described by the function $\sigma(\phi)$, Eq. (2.4), significant topographic diversity will certainly continue to apply, at least for this class of one-dimensional model potential energy functions. Indeed, the discrepancy between the $O(N)$ span for the potential energy [Eq. (2.5)],

and the number of modular units rising exponentially with N [Eq. (2.2)] offers increasing numbers of ways for up-and-down “folding” of the potential contour consistent with a given depth distribution. Consequently, significant kinetic diversity can be expected even under the constraint of fixed thermodynamic behavior. In particular the overall potential energy contour could be arranged to display a single metabasin as illustrated in Fig. 3(a), or a collection of many metabasins separated by high intervening barriers, Fig. 3(b).

The family of one-dimensional Φ 's thus far examined can be extended to include a no-net-rise basin unit $P(x|0)$. The resulting collection of composite Φ 's would then be encoded by spin-1 Ising sequences ($\mu_i=0, \pm 1$). The simple choice

$$P(x|0) = [\cos(2\pi x) - 1]/2 \equiv -\sin^2(\pi x) \quad (0 \leq x \leq 1) \quad (4.5)$$

conforms to the previous criterion of second-derivative continuity at the matching endpoints. However, the intrabasin partition function inevitably differs for this new basin shape (it can be expressed in closed form using the modified Bessel function I_0), thus requiring use of the averaging shown in Eq. (2.7) to determine f_{vib} . Including $P(x|0)$ as a modular unit removes the requirement that M be an even integer for periodic boundary conditions, but does not diminish the topographic diversity that can exist with a fixed basin depth distribution.

V. MULTIDIMENSIONAL GENERALIZATIONS

The principal and obvious shortcoming of the family of potentials defined above is that they are one-dimensional. By contrast, the dimension of the configuration space within which an N -body potential function exists is proportional to N . Therefore our next task is to extend the concepts thus far developed to a higher-dimensional format. The goal will be to demonstrate that a wide variety of geometrically and therefore kinetically distinct landscapes can all produce the same thermodynamics.

The simplest multidimensional extension involves a sum of separable contributions, Φ_i , each of the type defined in Sec. III above,

$$\Phi(x_1 \cdots x_n) = \sum_{i=1}^n \Phi_i(x_i). \quad (5.1)$$

The total number of basins (each one of which is n -dimensional) will be

$$M = \prod_{i=1}^n M_i. \quad (5.2)$$

We shall require that Φ satisfy periodic boundary conditions in each of the n directions.

The individual contributions Φ_i in Eq. (5.1) can be encoded by their own sequences of M_i Ising spins. And because topographic diversity exists in direction x_i for each i , at a fixed basin depth distribution, we can be assured that such diversity also exists for Φ . In fact, a single thermodynamic constraint on the depth distribution of the n -dimensional basins comprised in Φ , Eq. (5.1), is far less

limiting than a set of n basin-depth constraints applied to each of the Φ_i individually. Although the transformation rules stated at the end of Sec. IV are still relevant for each direction x_i , they can now be supplemented by other depth-distribution-preserving processes that operate simultaneously on two or more directions.

The separable form Eq. (5.1) implies that Newtonian dynamics on such an n -dimensional surface would consist of independent motions in each of the n directions. Small-amplitude motions close to a minimum in a realistic potential surface would always amount to essentially separable harmonic motions, but more generally the many-body dynamics would not be separable due to anharmonicity. Consequently a further extension of our family of model potentials to produce dynamic nonseparability is warranted. For this reason we now examine two-dimensional modular basin units defined over the unit square $0 \leq x, y \leq 1$. These modular units, to be denoted by $Q(x, y|a, b, c, d)$, will each have local maxima at the four-square vertices, saddle points along each square edge, and a single interior minimum. Furthermore, the normal derivative of each Q will vanish along the entire periphery of the unit square. The integer indices $a \cdots d$ will identify the individual Q 's by specifying their values at the square vertices,

$$Q(0, 0|\cdots) = a, \quad Q(1, 0|\cdots) = b, \quad (5.3)$$

$$Q(1, 1|\cdots) = c, \quad Q(0, 1|\cdots) = d.$$

This seems to be a more transparent notation for present purposes than a logically equivalent assignment of Ising spins to the square edges.

We shall restrict attention to cases in which the net change in each Q from one square vertex to an adjacent vertex is $0, \pm 1$. Some of the Q 's to be used are composed additively from the modular one-dimensional functions considered earlier, Eqs. (3.1), (3.2), and (4.5). Specific examples are the following:

$$Q(x, y|0, 0, 0, 0) = P(x|0) + P(y|0),$$

$$Q(x, y|0, 1, 1, 0) = P(x|+1) + P(y|0), \quad (5.4)$$

$$Q(x, y|0, 1, 2, 1) = P(x|+1) + P(y|+1).$$

Although each of these two-dimensional basins is internally separable, they can be combined with other modular units so that the resulting Φ is not separable overall. Rotation and reflection operations can be applied to the second and third of expressions (5.4) to generate other unit modular functions, such as $Q(x, y|0, 0, 1, 1)$ and $Q(x, y|2, 1, 0, 1)$.

Two other species of Q 's remain to be defined, neither of which is internally separable. They are $Q(x, y|0, 1, 0, 1)$ and $Q(x, y|0, 0, 1, 0)$. These species of course cannot be generated from the previous cases by rotation and/or reflection. We assign the following form to the first of these:

$$\begin{aligned}
 Q(x,y|0,1,0,1) = & -1/2 + (1/2)[\cos(2\pi x) + \cos(2\pi y)] \\
 & - (5/8)\cos(\pi x)\cos(\pi y) + (1/16) \\
 & \times [\cos(\pi x)\cos(3\pi y) \\
 & + \cos(3\pi x)\cos(\pi y)], \quad (5.5)
 \end{aligned}$$

which has the following interior minimum:

$$\begin{aligned}
 x_{\min} = y_{\min} = & 1/2, \\
 Q(x_{\min}, y_{\min}|0,1,0,1) = & -3/2. \quad (5.6)
 \end{aligned}$$

The other nonseparable species is

$$\begin{aligned}
 Q(x,y|0,0,1,0) = & -3/4 - (9/32)[\cos(\pi x) + \cos(\pi y)] + (1/2)[\cos(2\pi x) + \cos(2\pi y)] \\
 & + (1/32)[\cos(3\pi x) + \cos(3\pi y)] \\
 & + (5/16)\cos(\pi x)\cos(\pi y) - (1/32)[\cos(\pi x)\cos(3\pi y) + \cos(3\pi x)\cos(\pi y)]. \quad (5.7)
 \end{aligned}$$

This last function has a single interior minimum at

$$\begin{aligned}
 x_{\min} = y_{\min} \cong & 0.452\ 92, \\
 Q(x_{\min}, y_{\min}|0,0,1,0) \cong & -1.805\ 550\ 5. \quad (5.8)
 \end{aligned}$$

Figure 5 presents a picture of the modular surface defined by the function $Q(x,y|0,0,1,0)$.

The reader will notice that no $Q(x,y|0,1,1,1)$ -type species has been included in the definitions above. The reason is that such a modular unit cannot be expressed in the same simple trigonometric basis as shown for the other functions, under the same requirements of continuity and vanishing normal gradient at the perimeter of the unit square.

A composite $\Phi(x,y)$ satisfying periodic boundary conditions in x and y now can be created splicing together translated and elevated Q modules into an array of unit squares. The specific forms chosen for the Q 's guarantee that the resulting Φ and its gradient can be continuous at all shared square edges. We can formally set

$$\Phi(x,y) = Q(x-i, y-j|a_{ij}, b_{ij}, c_{ij}, d_{ij}) + K(i,j) \quad (5.9)$$

for that portion of the entire surface within the square,

$$i \leq x \leq i+1, \quad j \leq y \leq j+1, \quad (5.10)$$

for non-negative integers i, j that are subject to

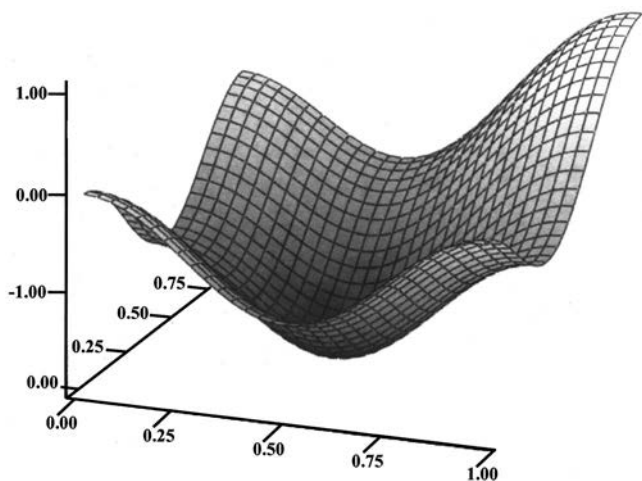


FIG. 5. Potential surface for the nonseparable basin function $Q(x,y|0,0,1,0)$, defined in Eq. (5.7).

$$1 \leq i \leq M_1, \quad 1 \leq j \leq M_2. \quad (5.11)$$

The integer constants $K(i,j)$ are analogous to the C 's in Eq. (3.8), providing the necessary elevation for the module. The selection of Q 's and K 's to form a composite Φ can be fully specified by the integer values of that Φ at the shared vertices of the network of squares.

Figures 6(a) and 6(b) present a simple nonseparable pair

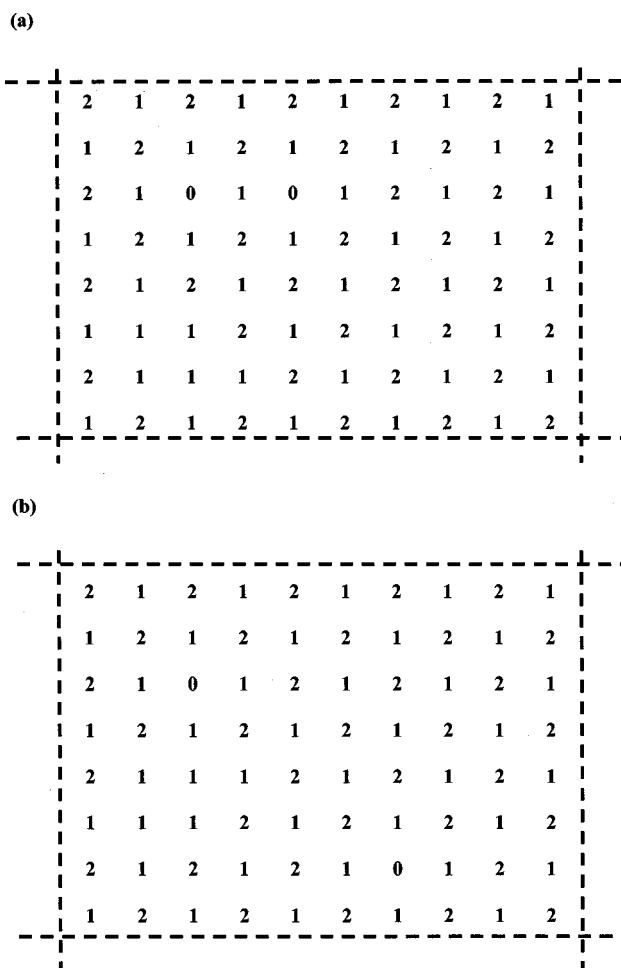


FIG. 6. A pair of nonseparable composite potentials that are thermodynamically equivalent but dynamically distinct. The respective two-dimensional modular units comprised in the Φ 's are specified implicitly by the integer values shown, equal to the local potential maxima at the shared square vertices. The horizontal and vertical dashed lines indicate the periodic boundaries.

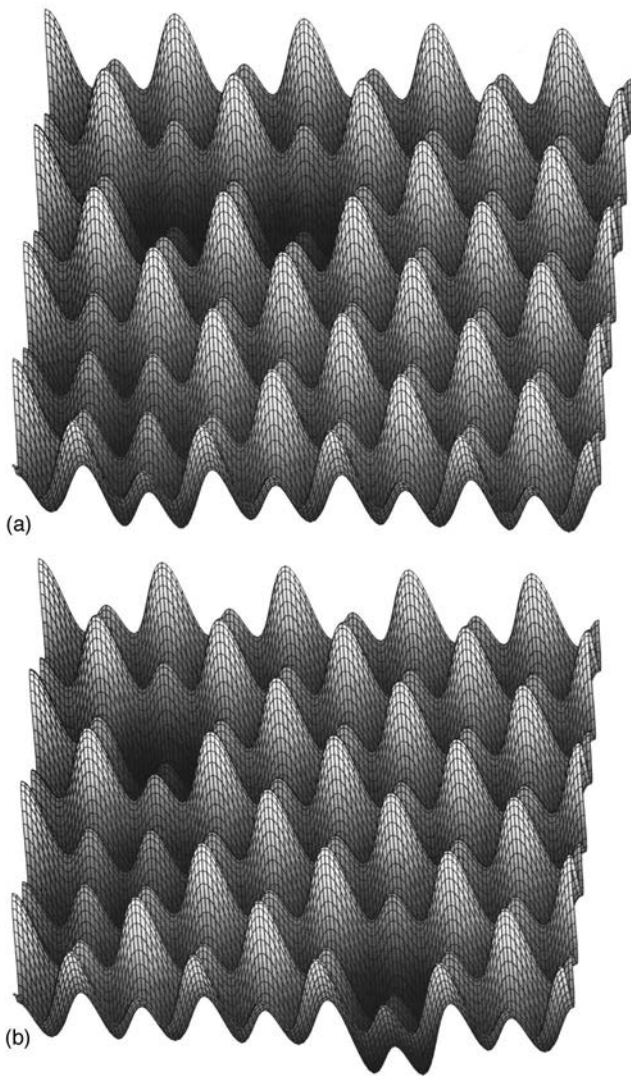


FIG. 7. Potential surfaces for the two thermodynamically equivalent composite potentials that were specified schematically in the prior Figs. 6(a) and 6(b).

of composite Φ 's that are thermodynamically equivalent, but dynamically distinct. These contrasting examples are symbolized in the figures by the 8×10 arrays of vertex values, as just described above. The reader can easily verify that the basin (module) enumeration by species and altitude is identical for Figs. 6(a) and 6(b), which indeed assures a common thermodynamic behavior. However the arrangements of those modules in the composite potential are distinct, specifically with different pathways between the lowest-lying minima that occur in the $Q(x,y|0,1,2,1)$ units. This latter feature surely influences and distinguishes the respective dynamical behaviors. Figures 7(a) and 7(b) present visual views of the corresponding potential surfaces.

Although the examples specified in Fig. 6 are transparent and obvious, it should be clear that with substantially larger M_1 and M_2 the opportunities would proliferate for widely disparate topographies that are thermodynamically "degenerate." In that respect this non-separable family of two-dimensional potentials is similar to the one-dimensional family described earlier in Secs. III and IV. Once again, for large

M , wide latitude will exist to vary the number and arrangement of metabasins without effecting the thermodynamics.

Two-dimensional, nonseparable functions of the kind just described can be combined to form a potential function in a higher number of dimensions in a manner analogous to that of Eq. (5.1),

$$\Phi(x_1 \cdots y_n) = \sum_{k=1}^n \Phi_k(x_k, y_k). \quad (5.12)$$

The Newtonian dynamics would then be partially separable into the n two-dimensional subspaces.

It should be clear that unit-cube or unit-hypercube modular functions could be defined and utilized in a straightforward generalization of the procedure followed for the one-dimensional and two-dimensional cases. Although this might produce rising technical complexity with increasing dimension of those modular units, it is hard to avoid the conclusion that the constraint of fixed thermodynamics would almost always be accompanied by dynamical diversity.

VI. CONCLUSIONS AND DISCUSSION

By using a modular basin approach, it has been possible to construct families of model "rugged landscape" potential energy functions. The simplest of these families involves one-dimensional functions, but multidimensional (and non-separable) generalizations have also been produced. A shared attribute of all of these families of model functions is their topographic diversity. In fact, the diversity is sufficiently pronounced that pairs of functions can be identified that share exactly the same thermodynamic behavior (depth distribution of potential energy minima), while differing drastically in those topographic attributes that control kinetic and relaxational behavior. The implication of these simple model results is that the same characteristic of kinetic diversity under the constraint of thermodynamic equivalence applies as well to the N -body case of real glass formers, where the dimension of the configuration space is $O(N)$, and the number of basins (in a symmetry sector) is exponentially large in N . A qualitatively similar conclusion about decoupling of thermodynamics and kinetics, based on a rather different view of the potential energy surface, appears in a recent paper by Wales and Doye.²⁶

Experimental observations of glassforming liquids have benefited from Angell's classification scheme between "strong" and "fragile" extremes. Although a few exceptions appear to exist, an empirical rule states that this classification simultaneously applies both to thermodynamic (calorimetric) and kinetic (flow and relaxational) properties, i.e., "strong" correlates with "strong," and "fragile" correlates with "fragile."²⁷ This empirical rule, and the success of the Adam-Gibbs equation, have focused attention on topographic features of the potential energy surface as possible sources of the apparent connection between thermodynamics and kinetics in supercooled liquids. However, the results obtained in this study seem to cast such speculation in a new and perhaps unexpected light. From the purely mathematical

standpoint illustrated by the model potential energy functions described above, thermodynamics would appear to be logically decoupled from kinetic behavior.

Several issues concerning our families of model functions need to be considered. First, all members of these families have upper bounds (remain finite), whereas realistic potential energy functions tend to become arbitrarily large at small interparticle separations. This qualitative discrepancy seems to be totally benign in the present context, though. System configurations with arbitrarily high potential energy are simply never visited during the temporal evolution of a many-body system. That part of the “rugged landscape” topography relevant to glass-forming behavior lies closer to the basin minima, and to the low-order saddle points that normally provide interbasin transitions.

A second issue that deserves consideration arises from the shapes of the unit modular regions out of which our composite potential energy functions have been constructed. Depending on the dimension of the space used, these are unit intervals, unit squares, unit cubes, etc., and they are placed together so as to tile the space in a nominally periodic fashion. However these shapes are a convenience, not a necessity. In an alternative development, it would have been possible to utilize other, less symmetrical, modular regions. Mixtures of differently-shaped modular regions selected to tile the space properly could also have been selected for use. Furthermore, inclusion of modular regions that are not just simply connected also appears to be feasible. Although each of these extensions might require additional technical complications, none of them appear to compromise the topographic flexibility present under the constraint of fixed thermodynamic behavior that characterize the examples developed above in Secs. III–V.

A third issue involves the shape of the large region over which the composite potential function is defined, and at the edges of which periodic boundary conditions have been imposed. This region is intended to mimic a single symmetry sector, as mentioned above in Sec. II. A realistic shape for such a symmetry sector would be highly nonconvex, and probably highly multiply connected. Nevertheless, no mathematical property arising from these complex features obviously intervenes in a continuation of our argument that thermodynamically identical potential energy functions can display widely divergent kinetic behaviors. We stress once again that this conclusion refers only to mathematical, not physical, characteristics of many-body potential energy functions.

Having made these claims, we are now obliged to confront the empirical linkage between thermodynamic and kinetic properties of glassforming substances, whereby the Angell classification scheme simultaneously assigns a “strong” versus “fragile” ranking to both groups of properties.^{4,27} It appears to us that the only viable option is to conclude that the empirical linkage arises not from a mathematical attribute of rugged potential energy surfaces per se, but from an additional physical principle that has had no role in constructing our model potential energy families. This principle presumably concerns the specific nature of interparticle interactions, arising from molecular shape, flexibility, ionicity,

covalent bond formation, etc. These interactions would have to give rise to a class of rugged energy landscapes in which drastically different multiple topographies (kinetic diversity) cannot in general arise from a single depth distribution (thermodynamics). It would be extremely useful to have in hand a clear and comprehensive statement of this additional principle, including the conditions under which exceptions could occur.²⁷ However the articulation of that principle is beyond the scope of the present paper.

Finally, we note that at least some glassformers appear to change their character from “fragile” at high temperature, to “strong” at low temperature.²⁸ This implies that the landscape topographies for such systems change qualitatively from those configuration-space regions preferentially occupied at high temperature, to those preferentially occupied at low temperature. The model potentials described in the previous sections of this paper could in principle be easily crafted to exhibit that kind of variable topography for thermodynamic or kinetic behavior, or both, but as before the two classes of attributes would be logically independent.

ACKNOWLEDGMENTS

The authors thank Mr. Vincent K. Shen and Dr. Karl Westerberg for assistance in preparing the figures for this paper. P.G.D. gratefully acknowledges support by the U.S. Department of Energy, Office of Basic Energy Sciences (Grant No. DE-FG02-87ER13714).

¹J. Jäckle, Rep. Prog. Phys. **49**, 171 (1986).

²C. A. Angell, Science **267**, 1924 (1995).

³P. G. Debenedetti, *Metastable Liquids* (Princeton University Press, Princeton, 1996), Chap. 4.

⁴C. A. Angell, J. Non-Cryst. Solids **131-133**, 13 (1991).

⁵W. Kauzmann, Chem. Rev. **43**, 219 (1948).

⁶(a) W. Nernst, *Nach. d. Ges. d. Wissensch. zu Göttingen, Math. phys. Kl., Heft I* (1906); (b) *Sitz.-Ber. d. preuss. Akad. d. Wiss.* (1906), Vol. 20; (c) M. Planck, *Treatise on Thermodynamics*, 3rd ed. (Dover, New York, 1945), pp. 272–292.

⁷Reference 3, pp. 250–253.

⁸F. H. Stillinger, J. Chem. Phys. **88**, 7818 (1988).

⁹D. Kivelson, S. A. Kivelson, X. Zhao, Z. Nussinov, and G. Tarjus, *Physica A* **219**, 27 (1995).

¹⁰G. P. Johari, J. Chem. Phys. **113**, 751 (2000).

¹¹G. Adam and J. H. Gibbs, J. Chem. Phys. **43**, 139 (1965).

¹²In Ref. 3, p. 257.

¹³F. H. Stillinger, Phys. Rev. B **32**, 3134 (1985).

¹⁴C. A. Angell, *Physica D* **107**, 122 (1997).

¹⁵A. Heuer, Phys. Rev. Lett. **78**, 4051 (1997).

¹⁶S. Sastry, *Nature* (London) **409**, 164 (2001).

¹⁷F. H. Stillinger, Phys. Rev. A **25**, 978 (1982).

¹⁸F. H. Stillinger, in *Mathematical Frontiers in Computational Chemical Physics*, edited by D.G. Truhlar (Springer-Verlag, New York, 1988), pp. 157–173.

¹⁹F. H. Stillinger, Science **267**, 1935 (1995).

²⁰F. H. Stillinger, J. Chem. Phys. **88**, 380 (1988).

²¹P. Häner and R. Schilling, *Europhys. Lett.* **8**, 129 (1989).

²²F. H. Stillinger, Phys. Rev. E **59**, 48 (1999).

²³O. M. Becker and M. Karplus, J. Chem. Phys. **106**, 1495 (1997).

²⁴D. J. Wales, J. P. K. Doye, M. A. Miller, P. N. Mortenson, and T. R. Walsh, *Adv. Chem. Phys.* **115**, 1 (2000).

²⁵C. L. Brooks III, J. N. Onuchic, and D. J. Wales, Science **293**, 612 (2001).

²⁶D. J. Wales and J. P. K. Doye, Phys. Rev. B **63**, 214204 (2001).

²⁷L.-M. Martinez and C. A. Angell, *Nature* (London) **410**, 663 (2001).

²⁸I. Saika-Volvod, P. H. Poole, and F. Sciortino, *Nature* (London) **412**, 514 (2001).